A Dissertation on

Decay of $^{228}Th^{*}$ formed using radioactive beam ^{132}Sn at above barrier energies

Dissertation submitted in partial fulfillment for the requirement of
The award of the degree of
Master of Science
In
PHYSICS

Under
The supervision of
Dr. Manoj K. Sharma
(Associate Professor)

Submitted by
Honey Mittal
Roll no: - 301004003

School of Physics and Materials Science
Thapar university
Patiala (Punjab) – 147004
July,2012

Dedicated To My Parents

Mentors and Friends

3

CERTIFICATE

I hereby certify that the work which has been presented in this thesis entitled, "**Decay of ^{228}Th* formed using radioactive beam ^{132}Sn at above barrier energies**" submitted in partial fulfillment of the requirements for the award of degree of **Master of Science** in **Physics** at **Thapar University, Patiala**, is an authentic record of my own work carried out under the supervision of **Dr. Manoj K. Sharma, Associate Professor, SPMS** and refers other researcher's work which are duly listed in reference section.

The matter embodied in this thesis has not been submitted for the award of any other degree of this or any other university.

Honey Mittal

Date: 13, July, 2012 (Honey Mittal)

This is to certify that the above statement made by the candidate is correct and true to best of my knowledge.

Msharma

Dr. Manoj Kumar Sharma
Associate Professor
SPMS, Thapar University
Patiala

Countersigned by:

dSingh

Dr. Kulvir Singh
(Professor & Head)
SPMS, Thapar University
Patiala

Dr. S.K.Mohapatra
Dean of Academic Affairs
Thapar University,
Patiala

Acknowledgement

I owe my deepest gratitude to **Dr. Manoj Kumar Sharma**, *my worthy supervisor,* without him the dissertation would not have been possible. I thank him for his patience and encouragement that carried me on through difficult times, and for his insights and suggestions that helped to shape my research skills. I express my sincere thanks to him for his valuable guidance in caring out under his effective supervision, encouragement and cooperation. His visionary thoughts have influenced me greatly. His dynamical attitude has empowered me with zeal of energy to conquer the miner details of my research work.

I also thank **Dr. Kulvir Singh, Professor** & Head, school of physics and material science for his support and providing facilities.

A special word of thanks to **Ms. Gurvinder Kaur**, research scholar for the help and valuable suggestions whenever I need it out for her busy schedule.

Special thanks to all my friends and the staff at the school of physics and material sciences for providing me a friendly atmosphere and encouraging me throughout this work. I am deeply thankful to my family, their moral support and patient has bared fruit through completion of this thesis.

Patiala
July,2012 Honey Mittal

Contents Page No.

List of Figures/Tables

Abstract

The reactions involving fusion of neutron-rich radioactive ion beam as projectile are of great interest in today's time. Since N/Z ratio is large, hence the complete fusion of projectile and target nuclei is not the only phenomenon observed in such reactions. Many other processes such as quasi-fission or incomplete fusion are also observed at times. The advantage of studying such systems is that with medium-mass, neutron-rich radioactive nuclei, the influence of neutron excess on fusion and compound nucleus dynamics can be explored, which helps us to improve our understanding on how to synthesize new neutron rich heavy nuclei. In this study, we have concentrated on the study of fusion-fission process only. We have investigated the decay of $^{228}Th^{*}$ formed in $^{132}Sn+^{96}Zr$ reaction at above barrier energies in order to analyze the effect of fusion of ^{132}Sn beam with ^{96}Zr target. The calculations have been done in the framework of Dynamical Cluster decay Model (DCM). We have calculated the fission cross-sections in reference to available experimental data. The effect of deformation and orientation is also seen. The decay has been analysed for spherical and the quadrupole (β_2) deformed choices of fragmentation. With both of these fragmentation choices, it has been seen that fission fragments are the major contributors towards the decay of $^{228}Th^{*}$ whereas evaporation residue contribute negligibly small. The calculated cross-sections compare nicely with the available experimental data. The fission fragment distribution is clearly asymmetric for spherical and β_2-deformed choices of fragmentation. However, at higher incident energies the symmetric fragments also start contributing, particularly for spherical case. The neck-length parameter "ΔR" decreases as a function of energy.

Chapter 1
Introduction

1.1Introduction

The study of nuclear structure and reactions forms an integral part of theoretical nuclear physics. Moreover, with advancement in the experimental field, the nuclear dynamics at extreme conditions of temperature, angular momentum, & energies are worth studying. Fusion is a process in which two nuclei are brought together to form a compound nucleus (CN). When these nuclei are enough close to each other then, there exists a substantial energy barrier, due to repulsion between the two nuclei, which opposes the fusion reaction. This energy barrier consists of the Coulomb and the nuclear potentials. However, the long range Coulomb repulsion between the nuclei is overcome by stronger, but short range, attractive nuclear force between these two nuclei. Actually the problem is to bring the nuclei sufficiently close so that the Coulomb barrier can be crossed over, say, via tunnelling. Hence, the two nuclei are required to collide with sufficient amount of kinetic energy to overcome their mutual electrostatic repulsion (or fusion threshold barrier) and subsequently, the role of strong but short range attractive nuclear force comes into play. In other words, the simplest picture of fusion is that of quantum tunnelling through a one dimensional barrier formed by long range Coulomb potential, the centrifugal potential and the short range nuclear potential. It means that the knowledge of interaction potential, forming barrier, between two nuclei is extremely important in order to have a systematic study of nuclear reaction. The mechanism of fusion of two heavy ions has been extensively investigated. The motivation for such studies is to understand the effect of entrance channel parameters, viz., energy, angular momentum and mass asymmetry, on the fusion process.

1.2 Heavy ion induced fusion-fission reaction

Nuclear fission process in which a nucleus divides into two fragments is one of the most interesting processes involving large scale collective nuclear motion. Since the discovery of

nuclear fission, extensive theoretical and experimental investigation have been carried out to understand the various aspects related to this phenomenon. Earlier the fusion-fission dynamics was carried out using neutron and α-particle beams. Later on, with the availability of the heavy ion accelerators, there was added impetus in the study of the dynamics of large shape changes in nuclear systems through the investigations of the nucleus-nucleus collisions involving fusion of two nuclei followed by fission process. These studies in nuclear physics, termed as nuclear macrophysics, encompass various aspects dealing with the statics, dynamics and statistical mechanics of nuclear systems. Heavy ion fusion-fission reaction paths are largely governed by the potential energy, impact parameter and the bombarding energy above the Coulomb barrier. For heavy ions ($Z > 2$) as the incident particles, the potential Coulomb barrier is higher than that for a proton, so the ion energy corresponding to one nucleon of the nucleus exceed a few MeV. The incident ions may not cause a nuclear reaction but may undergo elastic scattering in the field of Coulomb and nuclear forces. The angular distribution of ions upon elastic scattering exhibits diffraction characteristics. Generally, the energy dependence of effective cross sections for nuclear reactions by heavy ions are non resonant in nature. Elastic scattering is an exception. Nuclear reactions involving heavy ions are characterized by a large number of exit channels. For example, nuclei of Ca, Ar, S, Si, Mg, and Ne are formed upon the bombardment of $^{228}Th^{*}$ with ^{40}Ar ions. The following distinctions are made among nuclear reactions involving heavy ion reactions of nucleon transfer, reactions of the transfer of more complex particles, and merging reactions (formation of a compound nucleus). Nuclear reactions involving the transfer of a small number of particles or a small portion of energy are called soft collisions. The theory of such collisions has a great deal in common with the theory of direct reactions. Nuclear reactions involving the transfer of considerable mass or energy are called hard collisions, or deeply inelastic transfers. The angular distributions of the products of these nuclear reactions are sharply asymmetric and light products are formed in the decay process. The kinetic energy of the reaction products is close to the height of the exit Coulomb barriers and is virtually independent of the ion energy. A short-lived intermediate system is formed upon deeply inelastic collisions of nuclei. Despite the exchange of mass and energy, the nuclei of the intermediate system retain individuality as a result of tightly bound cores. Many new nuclides are formed as a result of hard collisions. In such reactions, compound nuclei with high excitation energies and angular momenta may arise. Nuclear reactions that involve the formation of compound nuclei are used in

the synthesis of trans-uranium elements (the combining of Pb and Bi target nuclei with corresponding heavy ion projectiles). A compound nucleus state formed in heavy ion collision is actually a quasi stable state with life time ~ 10^{-15} sec and it subsequently decays in the form of fission and evaporation residue (ER). The evaporation residue refers to nuclei with fragment mass equal to 1 to 4. In other words the nuclei with mass less than equal to alpha particle comprise the ER products. On the other hand fission refers to comparable fragmentation of compound nucleus (CN) state. Along with symmetric fission one may also have assymmetric fission, and in some cases the fission also can have contribution from heavy mass fragments HMFs and intermediate mass fragments IMFs. Here HMF corresponds to asymmetric fission fragments and IMFs are the decay products with mass 5 to 20.

1.3 Nuclear shell closure effect on decay of heavy nuclei

The Nuclear Shell Model has been studied and possesses some predictions in the region of lesser known super heavy elements. It predicts that the next doubly magic nucleus has atomic number Z = 114 or 120 or 126 and neutrons number N=178 or 184. This gives an indication of the existence of stable heavier elements in the island of stability. According to the Liquid Drop Model, the spontaneous fission barrier is nearly zero for heavy nuclei. But after the correction of the Shell Model of nuclear potential, the fission barrier of this elements is of relatively high of about 6 to 8 MeV. Subsequently, the half-life of these nuclei increases with respect to spontaneous fissions. The number of neutrons increase as we move above the periodic table and the nuclear deformation is expected to increase as neutron number increases. A super heavy nucleus is supposed to be formed if its half life time is greater than that of spontaneous fission life time, as expected for Z=114 or 120 or 126 and N=178 or 184 cases. This gives an indication, if super heavy nuclei have a high stability with respect to spontaneous fission, they will decay to their ground state through different other decays such as neutron decay, alpha decay and possibly beta decay. As in present case we intend to work [1] on $^{228}Th^{*}$, so the shell closures heavier than Z=82 and N=126 are involved in calculations. For present calculations we have taken Z=126 and N=184 as proton and neutron shell closures in super heavy region.

1.4 Deformed nuclei

Not all nuclei have the spherical shape with closed shells. In the heavy and super heavy mass region, nuclei have non spherical charge distributions even in their ground states. These deformed shapes govern the electric quadrupole moment. These nuclei are away or far away from closed shell with deformed shapes. These deformations include additional modes of nuclei to be in excited state with a possible change in of their electric quadrupole moment [2]**.**

Considering the distribution of the nuclear charge ρ(r), the multipole moment is important for determining the nuclear potential at any point p from a distance R away from the nuclear distribution of the nuclear charges as can be shown in figure 1.1.

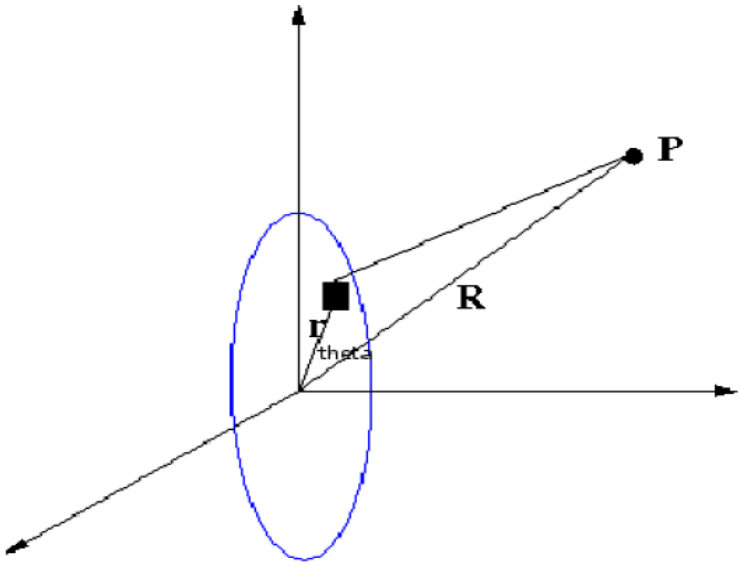

Fig.1.1 Potential of a quadrupole charge distribution

The potential at position P can be calculated as

$$V(\vec{r}) = \frac{1}{4\pi\varepsilon}\int \frac{\rho(\vec{r})}{\left|\vec{R}-\vec{r}\right|}d\vec{r} \qquad (1.1)$$

Using Taylor series expansion of the potential for small values of $\left|\vec{r}/\vec{R}\right|$ around the origin of the axis of the charge distribution, above equation reads as

$$V(\vec{r}) = \frac{1}{4\pi\varepsilon}\frac{q}{R} + \frac{1}{4\pi\varepsilon}\int \frac{\rho(\vec{r}) r\cos\theta}{R^2} d\vec{r} + \frac{1}{2}\frac{1}{4\pi\varepsilon}\int \frac{\rho(\vec{r})(3\cos^2\theta - 1) r^2}{R^3} d\vec{r} + \ldots\ldots \quad (1.2)$$

Now from fig 1.1

$$r\cos\theta = \frac{\vec{r}.\vec{R}}{R} = \sum_i x_i X_i / R_i \quad (1.3)$$

Where xi for i = 1, 2, 3 represent to the Cartesian coordinates. Expanding equation (1.2) in Cartesian coordinates, one can get

$$V(\vec{r}) = \frac{1}{4\pi\varepsilon}\frac{q}{R} + \sum_i \frac{\rho_i X_i}{4\pi\varepsilon_0 R^3} + \sum_{ij}\frac{1}{2}\frac{1}{4\pi\varepsilon_0 R^3}\frac{Q_{ij}}{R^5 X_i X_j} + \ldots\ldots \quad (1.4)$$

Where, $\rho_i = \int \rho(\vec{r}) x_i d\vec{r}$

And

$$Q_{ij} = \int \rho(\vec{r})(3x_i x_j - r^2\delta_{ij}) d\vec{r}$$

Here Q_{ij} is so called the quadrupole moment. If $Q_{ij} = 0$, the nuclear charges are distributed uniformly as sphere shape. If quadrupole moment is not equals to zero it give rise to two kinds of shape distributions.

1) It can cause a prolate deformation, making the spherical nucleus actually appear more like a football, positive quadrupole deformations.

2) It can cause an oblate deformation, making the spherical nucleus actually appear more like a doorknob, negative quadrupole deformations.

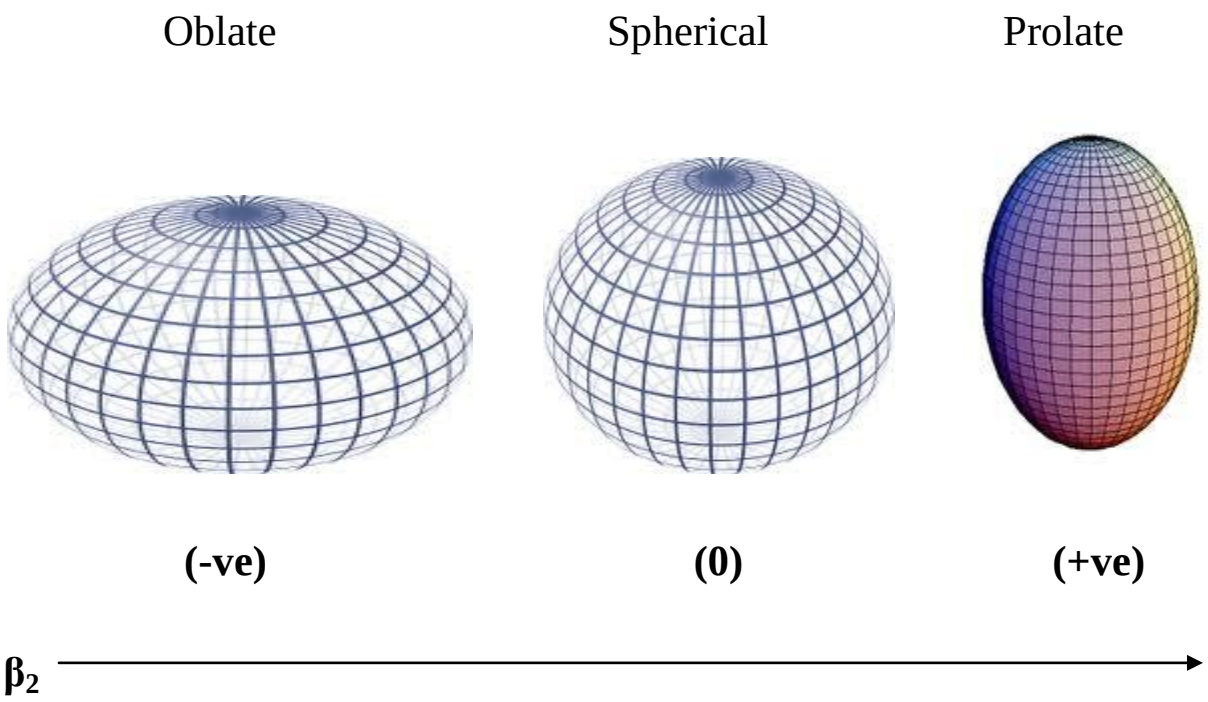

Fig.1.2 Nuclear shapes for oblate, spherical and prolate nucleus

The depth and the width of the capture well in the nucleus-nucleus interaction potential and the barrier height are supposed to play a dominant role in the dynamics of a compound nucleus. This feature is associated with the necessity to overcome the barrier that exists between two separated nuclei and with a formation of a scission neck between contacting nuclei in the capture well. Hence its indeed useful to study the influence of deformation and orientation on the nucleus-nucleus interaction potential. It has been observed that when we opt for a deformed target/ projectile combination for the synthesis of heavy/ super heavy nuclei the fusion probability in general gets increased as the barrier gets modified with inclusion of deformation & orientation effects**.** The apparent reason for this enhancement in fusion probability is that the inclusion of deformation and orientation effects of the colliding nuclei leads to lowering of its barrier height to provide easier path for compound nucleus formation. The collisions between deformed as well as oriented nuclei have been studied theoretically to establish the effect of deformation and orientation on fusion reactions [3]-[6].

1.5 Nuclear fusion reaction

Nuclear fusion is the process by which two or more atomic nuclei fuse together to form a single heavier nucleus. During this process, matter is not conserved because some of the mass of the fusing nuclei is converted into energy which is released. The binding energy of the resulting nucleus is greater than the binding energy of each of the nuclei that fused to produce it. The nuclear fusion has great potential as a sustainable energy source. This is due to the abundance of hydrogen on the planet and the inert nature of helium (the nucleus which would result from the nuclear fusion of hydrogen atoms). Although, a controlled nuclear fusion reaction has not yet been achieved, due to high temperatures required for sustaining such reactions. Some fusion techniques can be employed in the design of atomic weaponry and although more generally, it is fission and not fusion, that is associated with the making of the atomic bomb. The fusion of two nuclei with lower masses than iron generally releases energy, while the fusion of nuclei heavier than iron absorb energy. The opposite is true for the reverse process i.e. nuclear fission. This means that fusion generally occurs for lighter elements only, and likewise, that fission normally occurs only for heavier elements. There are extreme astrophysical events that can lead to short periods of fusion with heavier nuclei. This is the process that gives rise to nucleosynthesis, the creation of the heavy elements during events such as supernovae. From Figure 1.3, one can see that iron and nickel nuclei are the most stable nuclei and they have the largest binding energy per nucleon. Therefore, a fusion reaction of nuclei lighter than iron and nickel release energy and reactions of nuclei heavier than iron and nickel absorb energy. Nuclear fusion occurs naturally in stars and also has been made artificially but it is not completely controlled.

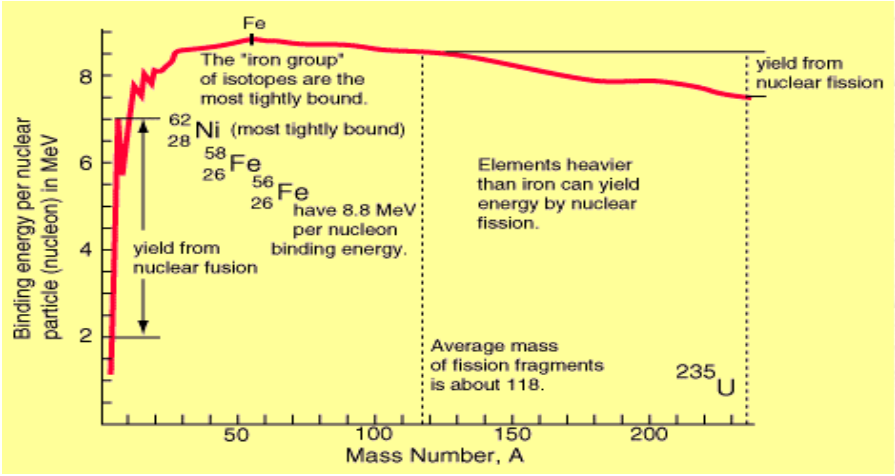

Fig.1.3 Binding energy per nucleon as the function of mass number

1.6 Fusion through neutron rich beams

The atomic nucleus is bound by the attractive short-range nuclear force that counters the repulsive Coulomb force. As the nuclear charge increases in heavier nuclei, the Coulomb force becomes dominant and eventually destabilizes the nucleus. Due to this reason one of the challenges in nuclear science is to use heavy-ion fusion reactions to find the heaviest elements. Measurements of fusion using neutron-rich radioactive beams are being used worldwide. The benefit of using neutron-rich radioactive nuclei, is that the influence of neutron excess on fusion and compound nucleus survival can impart many useful informations. This can improve our understanding on how to synthesize new neutron rich heavy nuclei. It is well known that heavy and super heavy nuclei are synthesized using heavy ion fusion reactions. The formation of a compound nucleus in heavy-ion fusion can be described schematically by two stages: capture and fusion. To achieve capture, the colliding nuclei are required to overcome the potential barrier generated by the nuclear and Coulomb forces. After capture, the composite system equilibrates its mass distribution and shape while evolving toward a compound nucleus shape. During this amalgamation, the composite system can separate into two massive fragments. This reaction is called fission and then competing CN processes like ER, IMF production etc. may also come in picture.

1.7 Compound nucleus formation

Neil Bohr in 1936 introduced the concept of a compound nucleus. When projectile and target come into close contact during a nuclear reaction, they form a combined system in which the nucleons interact strongly with each other. CN formation is a reaction in which two nuclei combine into a single excited nucleus, this excited nucleus lives for a relatively long time and "forgets" how it was formed . In a compound nucleus its observed that for a short range or abrupt sided potential there exist quasi-bound or virtual single particle states which have a positive energy. A long range potential like the Coulomb potential has no such states. The positive energy projectile particle is momentarily trapped in one of the single particle virtual states. Through collision with the nucleons inside the nucleus it shares its energy with them, raising some of them into excited states and itself dropping into one of these states. At CN stage all memory of the original mode of excitation is lost. Depending on the mass of CN the decay may consist of

various mechanisms. For light compound system with A_{CN} >> 40-80, the light particles(LPs) emission is always accompanied by intermediate mass fragments, the IMFs (with $2 < Z < 10$ and $5 < A < 20$). In this mass region the IMFs contribution is very small of the order of 5-10%, in comparison to LPs contribution. However, for the heavy compound systems $A_{CN} \approx 200$, the most probable decay mode of the compound nucleus is fission and heavy mass fragments (HMFs) ($20<A<A/2$), due to its instability against centrifugal repulsion, with small contribution from neutrons and γ-rays emissions. Beside this some non compound nucleus (NCN) decay can also be seen in the decay channel particularly for loosely bond reactions and then one associated with radioactive ion beams. This NCN component may comprise of quasi-fission (QF), incomplete fusion (ICF) etc.

In the present work, we intend to investigate the decay paths of $^{228}Th^{*}$ formed in $^{132}Sn+^{96}Zr$ reaction. It is relevant to mention here that ^{124}Sn is that last stable isotope of ^{124}Sn and ^{132}Sn is radioactive in nature. Also Z_pZ_t product of this reaction is much larger than 1600, therefore fusion hindrance effect [7-8] are supposed to be prominent in context of this reaction. However in present work we have addressed the capture cross-section of [1] and have tried to investigate the role of quadrupole deformations in decay of $^{228}Th^{*}$ nucleus. The calculations are performed by using Dynamical Cluster decay model (DCM), discussed in chapter 2. The calculated results and conclusion drawn are discussed in chapter 3.

References

[1] A. M. Vinod Kumar etal. Phys. Rev. C 78, 054608 (2008).

[2] Brain R Martin. Nuclear and Particle Physics, An introduction. John Wiley and Sons, Southern Gate, Chichester, West Sussex, England, (2006).

[3] R. K. Gupta etal. J. Phys. G: 31, 631 (2005).

[4] M. K. Sharma etal. J. Phy. G: Nucl.part.phys. 38, 055104 (2011).

[5] G. Sawhney, M. K. Sharma and R. K. Gupta Phy. Rev. C 83, 064610 (2011).

[6] M. K. Sharma etal. Phys. Rev. C 85, 064602 (2012).

[7] S. Bjørnholm and W. J. Swiatecki, Nucl. Phys. A 391, 471 (1982).

[8] W. J. Swiatecki, Phys. Scr. 24, 113 (1981); Nucl. Phys. A 376, 275 (1982).

Chapter - 2
Methodology

2.1 Introduction to DCM

The work presented in this thesis deals with the study of heavy ion reaction dynamics using the Dynamical Cluster-decay Model (DCM), which is used to study the decay of compound systems formed in low energy heavy ion reactions. The deformations and orientations degrees of freedom for reactants and products are dually incorporated in this model. Note that DCM [1-5] is a reformulation of PCM [6] for compound nuclei (CN). Both PCM and DCM originate from the Quantum Mechanical Fragmentation Theory, (QMFT) [7-9], based collective mass transfer processes. This model gives method of calculating the fragmentation potentials. Collective potentials and kinetic energy part of the Hamiltonian are discussed, together with the solution of the stationary Schrodinger wave equation. Here the decay of excited compound nuclei is studied as a collective clusterization process for emissions of the LPs, as well as the IMFs and HMFs, in contrast to the statistical models in which each type of emission is treated on different footing. Another advantage of using the DCM is that the structure effect of CN is also included via preformation of the fragments with relative probabilities.

In terms of the collective coordinates of mass asymmetry $\eta = A_1-A_2/A_1+A2$ and relative separation R respectively we get the nucleon-division between the outgoing fragments and the energy transfered can be calculated with the help of equation

$$E^*_{CN}=E_{c.m}+Q_{in=} \mid Qout \mid +TKE(T)+TXE(T) \qquad (2.1)$$

and the CN excitation E^*_{CN} in term of temperature T (in MeV) and is given by

$$E^*_{CN} = \frac{1}{9}AT^2 - T(Mev) \qquad (2.2)$$

DCM defines the decay cross-section, in terms of partial waves using the decoupled approximation to R and η–motions as

$$\sigma = \frac{\pi}{k^2}\sum_{l=0}^{\ell_{max}}(2l+1)P_0P \quad , \quad k = \sqrt{\frac{2\mu E_{c.m}}{\hbar^2}} \tag{2.3}$$

Where P_o is the preformation probability refering to η-motion and P is the penetrability refering to the R- motion. The structure information of the CN enters the model via preformation probability P_o of the fragments given by the solution of stationary Schrödinger equation in η at the fixed $R=R_a$

$$\left\{-\frac{\hbar^2}{2\sqrt{B_{\eta\eta}}}\frac{\partial}{\partial\eta}\frac{1}{\sqrt{B_{\eta\eta}}}\frac{\partial}{\partial\eta}+V_R(\eta,T)\right\}\psi^{\nu}(\eta)=E^{\nu}\psi^{\nu}(\eta) \tag{2.4}$$

With ν =0,1,2,3,….referring to the ground state and excited state solution . R_a is the first turning point of the penetrability path shown in figure 2.1 for $^{132}Sn+^{96}Zr$ reaction using β_2-deformation at ℓ=133 ħ. The potential V (R_a) acts like an effective Q-value, Q_{eff}, for the decay of the hot CN at temperature T, to two exit-channel fragments observed (T=0).

$$Q_{eff}\,(T) = B(T) - [\,B_L(T=0) + B_H(T=0)] = TKE(T) = V\,(R_a(T) \tag{2.5}$$

here B represents the binding energies.

The above defined decay of a hot CN into two cold (T=0) fragments, via Eq. (2.5), can be achieved only by emitting some light particle(s) (LPs), like n, p, α, or γ-rays of energy. By defining Q_{eff} (T) as in Eq. (2.5), in this model we treat the LP emission at par with intermediate mass fragments (IMFs) emission, beside this one can account for fission and heavy mass fragments (HMFs).

2.2 The scattering potential V(R)

For a given target projectile (A_1;A_2) combination, the scattering potential V(R) in Eq. (2.4) is defined as the sum of the temperature, deformations and orientations dependent Coulomb potential, proximity potential and angular momentum dependent potential, i.e.

$$V\,(R, T, \ell) = V_c(Z_i, \beta_{\lambda i}, \theta_i, T) + V_p(A_i, \beta_{\lambda i}, \theta_i, T) + V_l\,(R, A_i, \beta_{\lambda i}, \theta_i, T) \tag{2.6}$$

For spherical-plus-deformed nuclear collisions, only one orientation angle θ is enough, referring to the rotationally-symmetric deformed nucleus. $\Phi=0^0$for co-planar nuclei. For the decay of the hot compound nucleus, we use the postulate of first turning point

$$R_a=R_t+\Delta R(T) \quad \text{Where} \quad R_t= R_1+R_2 \tag{2.7}$$

Where ΔR(T) is the neck length parameter that assimilates the neck formation effects. This method is introducing a neck length parameter similar to that used in scission point and saddle point statistical fission models. The R_i are radius vectors which are also made temperature dependent can be calculated as

$$R_i(\alpha_i) = R_{0i}\left[1+\sum_{\lambda}\beta_{\lambda i}Y_{\lambda}^{(0)}(\alpha_i)\right] \tag{2.8}$$

$$\text{With, } R_{0i}(T) = 1.28A_i^{1/3} - 0.76 + 0.8A_i^{-1/3} \times (1 + 0.0007T^2) \tag{2.9}$$

In terms of $Q_{eff}(T)$, the second turning R_b satisfies (see Fig. 2.1)

$$V(R_a,\ell) = V(R_b, \ell) = Q_{eff}(T,\ell) = TKE(T) \tag{2.10}$$

With the ℓ-dependence of R_a defined by

$$V(R_a,\ell) = Q_{eff}(T,\ell = 0) \tag{2.11}$$

which means that the R_a, is the same for all ℓ -values, and that V (Ra, ℓ) acts like an effective Q-value, Q_{eff} (T, ℓ), given by the total kinetic energy TKE(T). Then, using (2.10), $R_b(\ell)$ is given by the ℓ-dependent scattering potentials, at fixed T .

Such a potential is illustrated in Fig.2.1 $^{132}Sn+^{96}Zr\rightarrow^{228}Th^*$, at ℓ =133ħ value. The second turning point R_b is marked for the ℓ =133ħ case of $R_a = R_t + \Delta R(T)$. The decay path for the ℓ=133ħ begins at $R = R_a$.

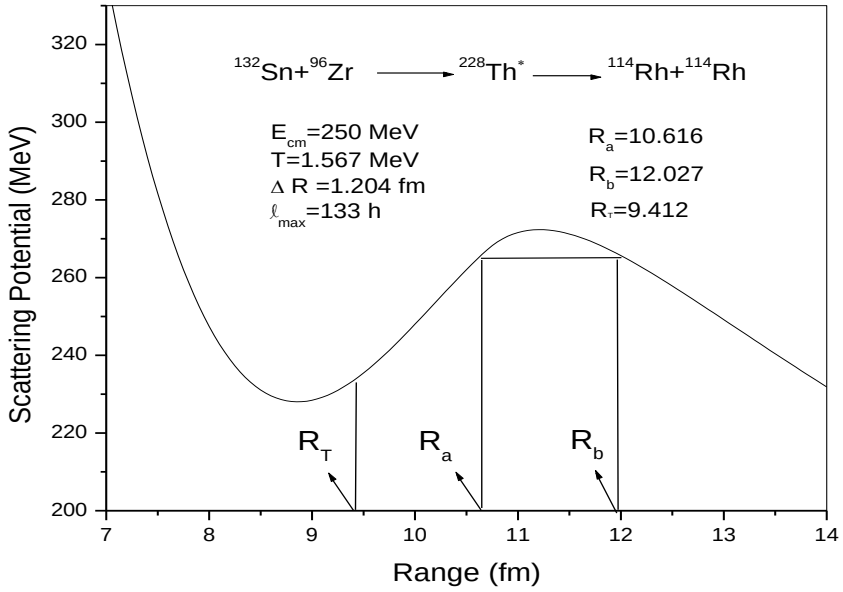

Fig.2.1. Scattering Plot for $^{132}Sn+^{96}Zr \rightarrow ^{228}Th^{*}$ reaction

2.3 The fragmentation potential V(η)

The fragmentation potential V(η,R) is shown as

$$V_R(\eta,T) = \sum_{i=1}^{2}\left[V_{LDM}(A_i,Z_i,T)\right] + \sum_{i=1}^{2}\left[\delta U_i\right]\exp(-T^2/T_0^2) + V_c(R,Z_i,\beta_{\lambda i},\theta_i,T) + V_p(R,A_i,\beta_{\lambda i},\theta_i,T) + V_l(R,A_i,\beta_{\lambda i},\theta_i,T)V_R(\eta,T) \quad (2.12)$$

The fragmentation potential V (η), appearing in equation (2.12) is calculated at a fixed distance $R = R_1 + R_2 + \Delta R$ for consideration of deformed and oriented reaction product.

2.4 The nuclear proximity potential

When a nucleus is at the verge of dividing into two fragments, then the two surfaces actually face each other across a small gap or crevice. In such situations, the surface energy term alone could not give rise to the strong attraction that is observed when the two surfaces are brought in close

proximity. These additional attractive forces are called proximity forces and the additional potential due to these forces is called the nuclear proximity potential.

Blocki etal. [10] have reanalyzed and extended a theorem, originally due to Deryagin [11], according to which the force between two gently curved surfaces in close proximity is proportional to the interaction potential per unit area between the two flat surfaces. The original expression of Blocki based on the pocket formula was for spherical nuclei, and is given as

$$V_P(s_0) = 4\pi \bar{R}\, \gamma b \Phi(s_0) \tag{2.13}$$

Where $\Phi(s_0)$ is the universal function, independent of the shapes of nuclei or the geometry of nuclear system, but depends on the minimum separation distance

$$\Phi(s_0) = \begin{cases} -\frac{1}{2}(s_0 - 2.54)^2 - 0.0852(s_0 - 2.54)^3 \\ -3.437\exp\left(-\frac{s_0}{0.75}\right) \end{cases} \tag{2.14}$$

respectively, for $s_0 \leq 1.2511$ and $s_0 \geq 1.2511$. Here, s_0 is defined in units of b, i.e. s_0 is s_0/b. This function is defined for negative (the overlap region), zero (touching configuration) and positive values of s_0. For a fixed R, the minimum distance s_0 for spherical nuclei is defined as

$$s_0 = R - R_1 - R_2 \tag{2.15}$$

where $R = 1.07A_i^{1/3}$(i=1,2). b is the diffuseness of the nuclear surface given by

$$b=[\pi/2\sqrt{3}\ln 9]_{t10\text{-}90} \tag{2.16}$$

where $t_{10\text{-}90}$ is the thickness of the surface in which the density profile changes from 90% to 10%. The value of b ~1 fm. The γ is the specific nuclear surface tension given by

$$\gamma = 0.9517[1\text{-}1.7826(N\text{-}Z/A)^2] \text{ Mev fm}^{-2} \tag{2.17}$$

R' is the mean curvature radius of the reaction partners, characterizing the gap, which for spherical nuclei is given by

$$\overline{R} = R_1R_2 / R_1 + R_2 \tag{2.18}$$

2.5 The Coulomb potential

The Coulomb potential describes the force of repulsion between two interacting nuclei due to their charges. It acts along the line joining of two nuclei. The Coulomb potential for two interacting spherical nuclei is given as

$$V_c = Z_1 Z_2 e^2 / R \tag{2.19}$$

For interacting deformed and oriented nuclei, the Coulomb interaction reads as

$$V_C(Z_i, \beta_{\lambda i}, \theta_i, T) = \frac{Z_1 Z_2 e^2}{R(T)} + 3Z_1 Z_2 e^2 \sum_{\lambda, i=1,2} \frac{R_i^{\lambda}(d_i, T)}{(2\lambda+1)R(T)^{\lambda+1}} \tag{2.20}$$

In this expression, the quadrupole-quadrupole interaction term, proportional to $\beta_{21}\beta_{22}$, is neglected since it has a short-range character. For nuclei lying in the same plane we have generalized it to include the higher order deformations ($\lambda = 3, 4...$), obtaining

2.6 Solution of the Schrodinger equation and preformation probability (P_0)

The Schrodinger equation in mass fragmentation co-ordinate η can be solved using the appropriate Hamiltonian. On solving numerically, $|\psi^{v}(\eta)|^2$ gives the probability P_0 of finding the mass fragmentation η at a fixed R on the decay path.

$$P_0(A2) = |\psi^{v}(A2)|^2 \tag{2.21}$$

It is relevant to mention here that for fission studies, the motion in R at the saddle point is adiabatically slow as compared to the η motion. Therefore, the potential is minimized in the neck and deformation coordinates β_1 and β_2 at each R and η values. Starting from the nuclear ground state in spontaneous fission or cluster decay, and to have complete adiabaticity, only the lowest vibrational state $\nu = 0$ is occupied. The mass (or charge) distribution yield, proportional to the probability $|\psi^{(0)}(\eta)|^2$ or $|\psi^{(0)}(\eta_z)|^2$ of finding a certain mass (or charge) fragmentation η (or η_z) at a position R on the decay path, when scaled to fragment mass A_2, ($d\eta = 2/A$) is given by:

$$Y(A_2) = \left|\psi_R^{(0)}(A_2)\right|^2 \frac{2}{A}\sqrt{B_{\eta\eta}(A_2)} \tag{2.22}$$

Now, if the system is excited or we allow interaction between various degrees of freedom, higher values of *v* would also contribute. These enter via the excitation of higher vibrational states, and through the temperature dependent potential V and masses $B_{ij.}$ Note that we are dealing here with a directly measurable quantity, the mass (or charge) asymmetry, which works dynamically as mass (or charge) transfer coordinate. Thus, the calculated yields Y (A_i) (or Y (Z_i)) are directly comparable with experiments. The nuclear shape, once minimized in the neck and deformation coordinates β_1 and β_2 at a given R (=R_{saddle}), remains fixed for both the mass and charge distributions of fission or decay fragments which is decided in reference to neck-length parameter "ΔR".

2.7 Penetration probability (P)

Penetrability P measures the capability of fragments nucleus to penetrate the potential barrier generalized during compound nucleus formation. The penetrability P is the WKB integral between R_a and $R_{b.}$

$$P = \exp\left[\frac{-2}{h}\int_{R_a}^{R_b}\{2\mu[V(R) - Q_{eff}]^{\frac{1}{2}}\,dR\}\right] \tag{2.23}$$

Here first turning point is given as:

$$R_a = R_t + \Delta R(T) \tag{2.24}$$

Where R_t is the touching point, also shown in figure 2.1. It may be noted that R_a, given in eqn.2.24 is same for all ℓ-values.

References

[1] R. Kumar & M. K. Sharma Phys. Rev. C 85, 054612 (2012) ; D. Jain, R. Kumar, M. K. Sharma & R.K Gupta, Phys. Rev. C 85, 024615 (2012).

[2] M. K. Sharma, G. Sawhney, R. K. Gupta, W. Grenier, J.Phys.G:Nucl.Part.Phys. 38 105101 (13pp) (2011); K. Sandhu, M. K. Sharma, R. K. Gupta, Phys. Rev. C 85 024604 (2012).

[3] B. B. singh. M. K. Sharma and R. K. Gupta, Phys. Rev. C 77 054613 (2008); M. Kaur, R. Kumar and M. K. Sharma Phys. Rev. C 85 014609 (2012); M. Kaur, M. K. Sharma Phys. Rev. C 85 054605 (2012).

[4] R. K. Gupta, M. Balasubramaniam, R. Kumar, N. Singh, M. Mahhas, and W. Greiner, J. Phys. G: Nucl. Part. Phys. C 31, 631 (2005); M. Manhas and R. K. Gupta, Phys. Rev. C 72, 024606 (2005).

[5] R. K. Gupta, M. Manhas, G. MÄunzenberg, and W.Greiner, Phys. Rev. C 72, 014607 (2005).

[6] S. S. Malik & R. K. Gupta Phys. Rev. C 39, 1992 (1989).

[7] J. Maruhn and W. Grenier, Z. Phys. 251, 431 (1972).

[8] R. K. Gupta and W. Grenier, in Heavy Elements and Related New Phenomena, edited by W. Grenier and R. K. Gupta, Vol. I (World Scientific, Singapore, 1999).

[9] R. K. Gupta, M. K. Sharma, S. Singh, R. Nouicer and C. Beck, Phys. Rev. C 56, 3242 (1997); R. K. Gupta, M. K. Sharma, N. V. Antonenko and W. Scheid, J. Phys. G: Nucl. Part. Phys. 25, L47 (1997); M. K. Sharma, R. K. Gupta, and W. Scheid, ibid. 26, L45 (2000).

[10] J. Blocki, J. Randrup, W. J. Swiatecki, and C. F. Tsang, Ann. Phys. (NY) 105, 427 (1977).

[11] Deryagin, Kolloid Z. 69, 155 (1934).

Chapter 3
Results and Discussion

3.1 Introduction

The study of fusion reaction induced by a n-rich radioactive beam is of great use for the synthesis of heavy and superheavy elements. So, with an aim of having information related to nuclear structure and dynamics of nuclear systems, the fusion of massive nucleus ^{132}Sn with ^{96}Zr target has been studied. The experimental data [1] for cross-section of ^{228}Th* has been reported over a wide range of incident energies (above the coulomb barrier), and the same has been tested in the framework of DCM [2-6]. The decay of ^{228}Th* has been studied and we observe that the fission fragments form a dominating part of cross-section whereas evaporation residue(ER) contribution is negligibly small as has been reported in experimental data [1]. The cross-sections have been fitted within one parameter of DCM i.e. the neck-length parameter ΔR and are summed up to $\ell = \ell_{max}$, where l_{max} is chosen at point for which $\sigma_{ER} \longrightarrow 0$. To see the effect of deformations and orientations, the calculations have been done with spherical and β_2 deformed choice of fragmentation. The level density parameter used for these calculations is $a=A_{CN}/9$, as already mentioned in chapter 2. This chapter contains the details of DCM calculations imparting information about fragmentation path of ^{228}Th* nucleus. In the beginning, the comparison at both the extreme values of energy i.e. the minimum centre-of-mass energy E_{cm} =193 MeV and maximum E_{cm} =250 MeV has been done. In addition to this, the comparison for spherical and deformed fragmentation choices is also explained in detail. The cross-section reported in [1] are the capture cross-section which is considered to be the sum of evaporation residue (ER), fission fragments and the quasi-fission (QF) fragments. i.e.

$$\sigma_{capture} = \sigma_{ER} + \sigma_{fission} + \sigma_{QF}$$

The ER cross-section calculated using DCM are observed to be negligible of the order of micro barn in agreement with experimental results. So far as fission cross-section is concerned it dominates the total cross-section. But the individual contribution of QF has not been accounted because the channel that signifies the QF comes in the domain of fission fragments itself. It may

be noted that fragments in the range 84-103 contribute towards fission cross-sections and one of the reaction partner ^{96}Zr comes within this range. As in quasi-fission, it is believed that interacting particles do not loose their identity in decay channel, so one may presume that QF component is contributing towards fission decay in context of present calculations. Thus, in DCM the major contribution towards the decay of ^{228}Th* is from fission process. Although calculations have been done at all reported energies but fragmentation behaviour is shown for only two extreme energies. These results are discussed ahead with possible explanation of figures.

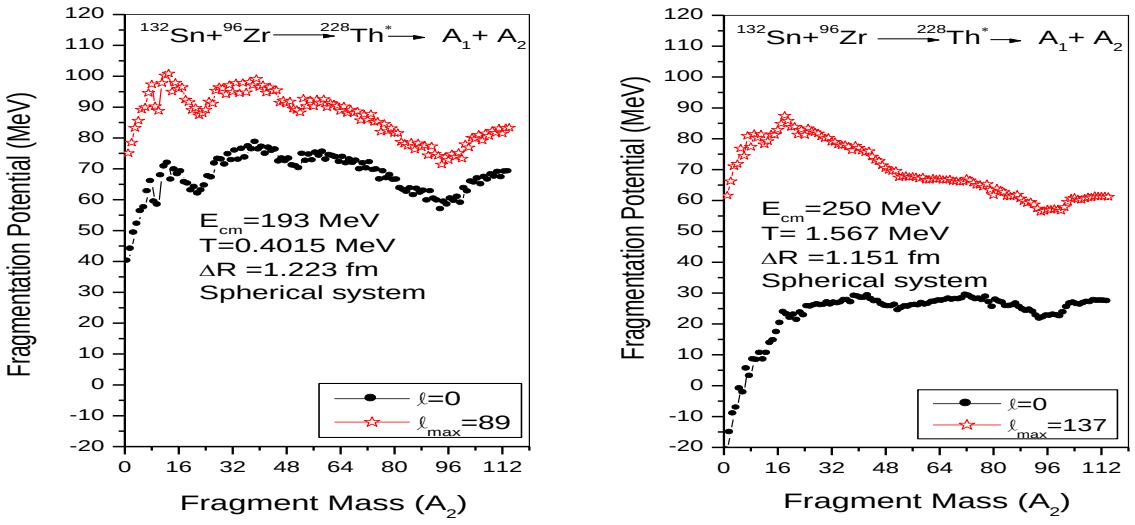

Fig.3.1 Fragmentation potential as the function of fragment mass (A_2) for spherical fragmentation at (a) E_{cm}=193 MeV and (b) E_{cm}=250 MeV.

Fig.3.1 shows the fragmentation potential as a function of fragment mass at ℓ =0 and $\ell = \ell_{max}$. In this figure comparison of fragmentation potential at E_{cm}=193 MeV and E_{cm}=250 MeV has been done by taking spherical approach into account. The neck-length parameter ΔR for E_{cm}=193 MeV is 1.223 fm and for E_{cm}=250 MeV is 1.151 fm. This shows that the ΔR values are higher at minimum energy and decrease with increase in energy. Interestingly the fragmentation path shows some variation while going from lower E_{cm} value to higher one. At lower E_{cm} value the fragmentation is clearly asymmetric, whereas the symmetric fragments starts emerging at higher E_{cm} values.

The contribution fragments for fission process lie in the range of (A/2 $\pm$ 20). Precisely the dominating fragments at minimum energy, range from 90-101 whereas, at maximum energy the range changes to 89-103.

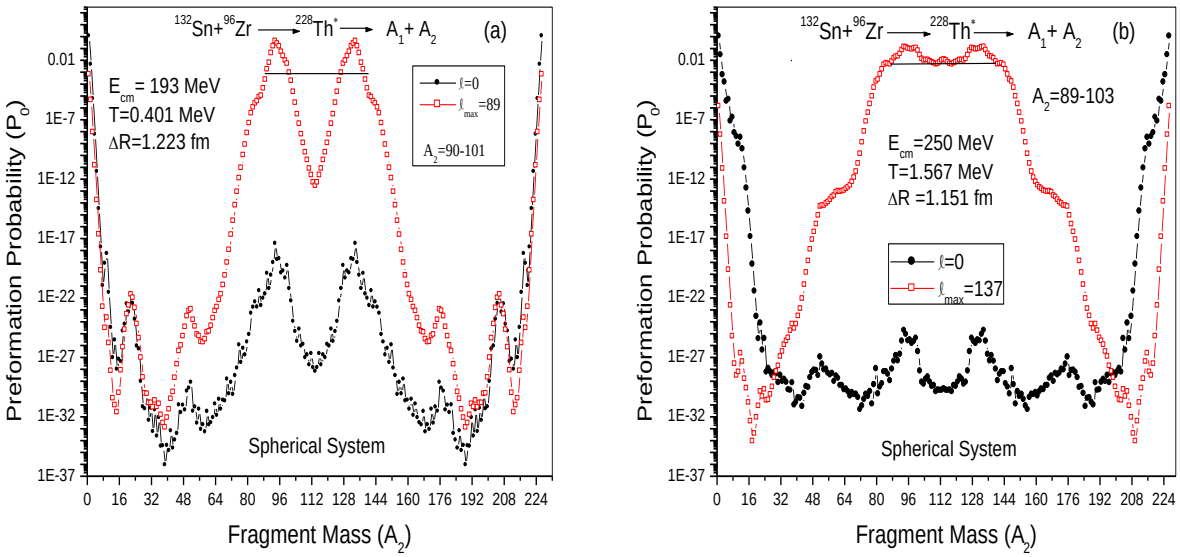

Fig.3.2 Preformation probability as the function of fragment mass for spherical fragmentation at (a) E_{cm} =193 MeV and (b) E_{cm} =250 MeV

The variation of preformation probability P_0 as the function of fragment mass A_2 is shown in fig.3.2. The figure 3.2 shows a comparison at both the extreme energies i.e. at minimum value of E_{cm} =193 MeV and maximum value of E_{cm} =250 MeV. With the change in energy the magnitude of P_0 changes. It increases with increase in energy. The maximum angular momentum value (ℓ_{max}) at which $\sigma_{ER} \longrightarrow 0$ is 89ħ for minimum energy and 137ħ for maximum energy. The neck-length parameter ΔR decreases contrary to ℓ_{max} value. It is 1.223 fm for E_{cm}=193 Mev and decreases to 1.151 fm for E_{cm}=250 MeV. At lower centre-of-mass energy, asymmetric fission fragments contribute more towards the fission cross-section. Whereas at higher energy the contribution of symmetric fission fragments become comparable to asymmetric ones. This behaviour is more prevalent at $\ell = \ell_{max}$ case.

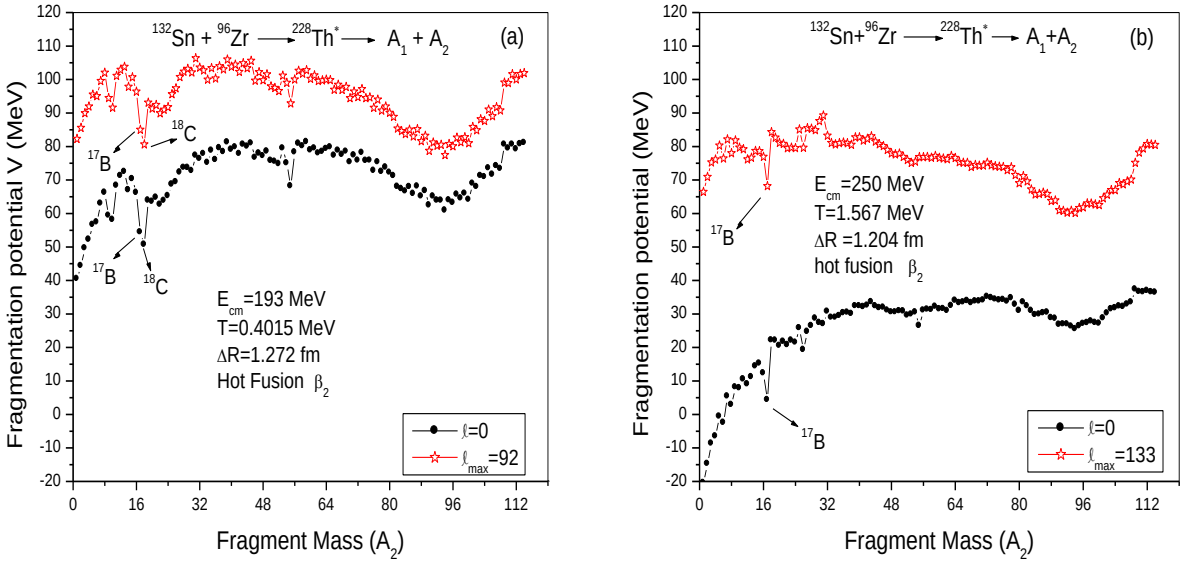

Fig.3.3 Fragmentation potential as the function of fragment mass (A_2) for β_2-deformed fragmentation for compound system $^{228}Th^*$ at (a) E_{cm}=193 Mev (b) E_{cm}=250 MeV.

Fig. 3.3 shows the fragmentation potential as a function of fragment mass at the ℓ =0 and ℓ = ℓ_{max} for β_2-deformed case. The sharp minima at ^{17}B and ^{18}C shows the preference for these clusters. However, it has been observed that the penetrability of this cluster is extremely small so the dips at ^{17}B and ^{18}C do not contribute much towards DCM calculations. In this figure comparison of fragmentation potential at E_{cm} =193 MeV and E_{cm} =250 MeV the respective ΔR values are 1.272 fm and 1.204 fm. This shows the ΔR values are higher at minimum energy and decrease with increase in energy. Moreover, the ℓ_{max} is also different from that of spherical approach. The potential energy surface for both energies are almost same with only difference in the magnitude of fragmentation potential and asymmetric fragmentation seems to be operating similar to the one observed for spherical case at low energy.

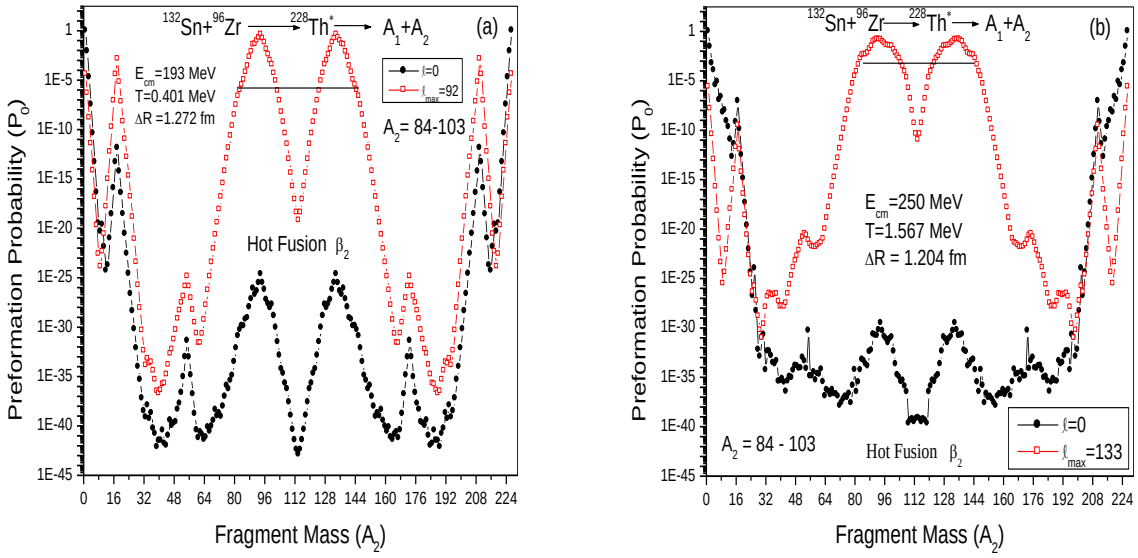

Fig. 3.4 Variation of Preformation probability as the function of mass fragments $A_i(i=1,2)$ for β_2-deformed system at (a) E_{cm} =193 Mev and (b) E_{cm}=250 MeV.

The Preformation graph is plotted at ℓ=0ħ and ℓ= ℓ_{max} for minimum and maximum energies. The fragments corresponding to ℓ_{max} contributing to fission decay are 84-103. From figure 3.4 we may observe that at minimum ℓ-value i.e. ℓ=0ħ the contribution of LPs (evaporation residues) dominate as compared to fission fragments. But the trend is no more same at maximum ℓ-value i.e. ℓ_{max} . For both the extreme energies, the fission contribution starts dominating at higher ℓ-values and consequently the fission fragments are prominent and ER are negligibly small. With β_2-deformed choice of fragmentation the fission distribution is clearly asymmetric independent of energy of incident beam.

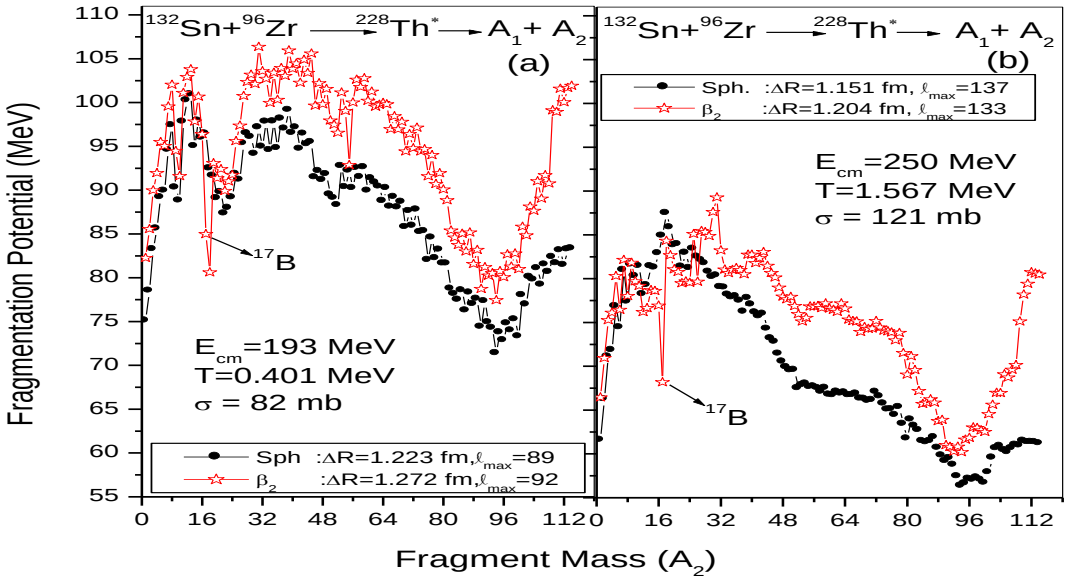

Fig.3.5 Fragmentation potential as the function of fragment mass (A_2) for decay of $^{228}Th^*$. The behaviour is shown for spherical and β_2-deformed choice of fragmentation at (a) E_{cm}=193 MeV and (b) E_{cm}=250 MeV.

The comparison of structural behaviour of spherical and quadrupole (β_2) deformed consideration is shown in fig.3.5. The role of deformation is prominent from these figures. As is clear, from figures (a) and (b) that the magnitude of potential is different at both energies. It is less for the fragments at higher energy i.e. E_{cm}=250 MeV. This lower potential supports the view, that cross-sections at higher energy are more as compared to E_{cm}=193 MeV. The structure for spherical and β_2-deformed approach is almost similar for LPs and fission fragments. A small change in behaviour is observed in mass lying between intermediate mass fragment (IMF) and heavy mass fragment (HMF) range. The neck-length parameter ΔR, that fits the cross-section at these energies, shows a similar trend in going from spherical to β_2-deformed choice. It's greater for deformed systems independent of energy of incident beam. The fragmentation potential rises for deformed system as a result of which the neck-length parameter needs to be increased as compared to spherical approach.

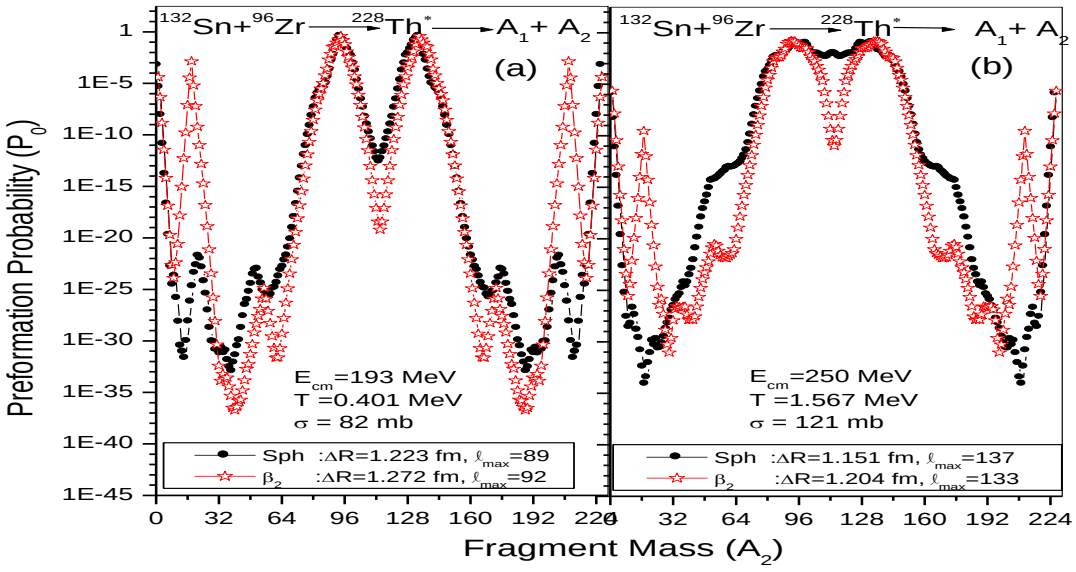

Fig. 3.6 The comparison of preformation probability (P_0) as the function of fragment mass A_i (i=1,2) for spherical and β_2-deformed choices at extreme energy conditions. (a) E_{cm}=193 MeV and (b) E_{cm}=250 MeV.

The preformation probability P_0 for the decay of $^{228}Th^*$ formed in $^{132}Sn+^{96}Zr$ reaction is plotted as a function of fragment mass (A_i, i=1,2). These figures help us to clearly identify the role of quadrupole deformation and spherical approach. The comparison at both the energies is carried out at maximum value of angular momentum i.e. ℓ_{max} only. It is observed from fig.3.6(a) that deformations play a role in intermediate mass fragments (IMF) region, but its behaviour is almost same as that of spherical approach for heavy mass fragments (HMF) and fission fragments and LPs. But the same is not true for higher energy, where preformation probability P_0 is almost symmetric for spherical choice of fragmentation.

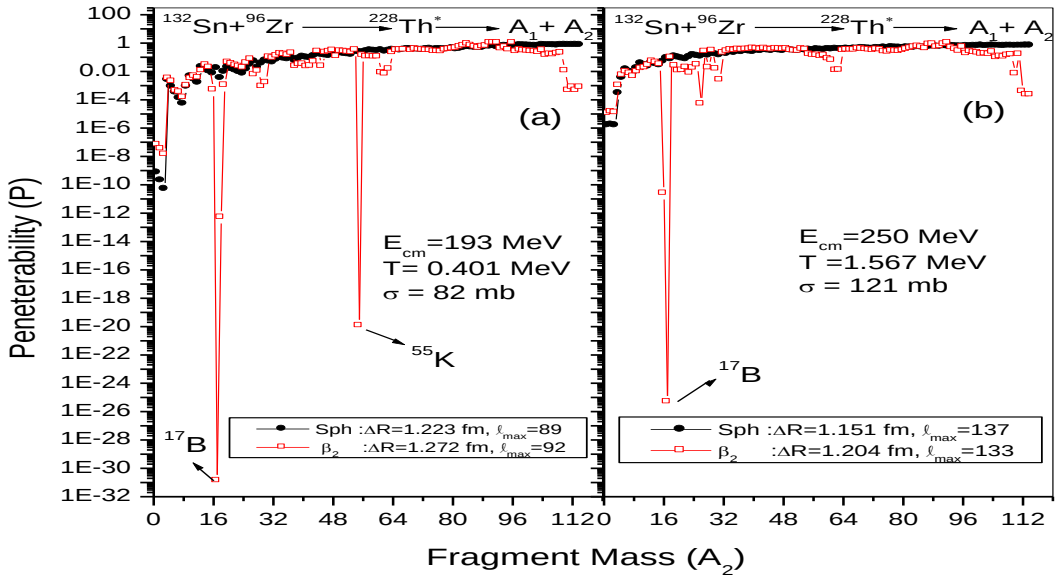

Fig.3.7 Penetrability as the function of fragment mass for spherical and β_2-deformed system at (a) E_{cm}=193 MeV and (b) E_{cm}=250 MeV.

Fig.3.7 shows penetrability (P) as a function of fragment mass (A_2) for spherical and quadrupole deformed choice of fragments. The variation is shown at ℓ_{max} value for both energies. The penetrability remains almost constant for spherical fragmentation, but with β_2 deformation included certain major dips are observed. The fragments identified at these dips, are ^{17}B,^{18}C and ^{55}K. It is to be recalled that in fig.3.5 a similar dips we observed for same fragments. Hence the enhanced probability of these fragments gets counter balanced by small penetration probability and hence they do not contribute much towards capture cross-section. It may be noted that a dip at ^{55}K is observed at low energy, but the same is not there at higher energy. As a result the contribution of ^{55}K towards cross-section would be less.

$E_{cm(MeV)}$	$E_{CN(MeV)}$	$\ell_{max(\hbar)}$	T(MeV)	ΔR(fm)	σ_{DCM}		$\sigma_{Expt\ (mb)}$
					$\sigma_{fission(mb)}$	$\sigma_{ER\ (\mu b)}$	
193	3.6835	92	0.4015	1.272	82.8	0.01	82
201	11.6835	109	0.6991	1.250	175.4	0.36	177
208	18.6835	120	0.8787	1.216	147.2	1.94	148
218	28.6835	126	1.0839	1.228	204	7.47	204
229	39.6835	131	1.2714	1.209	171	9.38	171
239	49.6835	132	1.4203	1.214	162	10.9	162
250	60.6835	133	1.5675	1.204	121.4	9.05	121

Table 3.1 DCM calculated fission cross-section compared with experimental cross-sections [1] for decay of $^{228}Th^{*}$ formed in $^{132}Sn+^{96}Zr$ reaction at all energies, with quadrupole (β_2) deformation.

The variation of neck-length parameter ΔR as a function of centre-of-mass energy E_{cm} for the decay of $^{228}Th^{*}$ is shown in fig.3.8 and also tabulated in table.3.1. With increase in energy the neck-length parameter decreases. Although, the variation is very small towards the higher end of energy. The variation of neck-length parameter ΔR is represented by the following second order polynomial equation in terms of E_{cm}.

$$\Delta R = 2.80 - 0.01 * E_{cm} + 2.78E - 5 * E_{cm}^{2}$$

For the neck-length parameter ΔR values depicted in fig.3.8, the available cross-sections of [1] are fitted nicely in the framework of DCM, as shown in table 3.1 and fig 3.9.

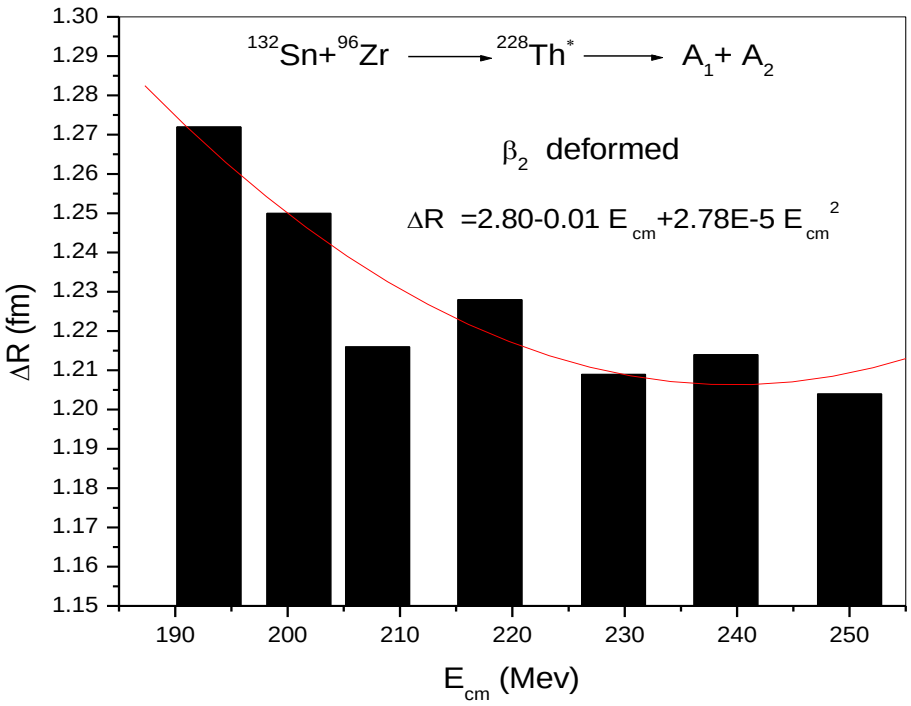

Fig. 3.8 Neck length parameter ΔR as a function of E_{cm} for $^{132}Sn+^{96}Zr$ reaction. The ΔR shown here is corresponding to quadrupole deformation.

Now, we compare the cross section calculated by DCM Model and experimental cross section. The cross-sections are plotted at seven different energies E_{cm} =193,201,208,218,229,239,250 MeV. Results obtained by DCM model has very small deviation from Experimental cross-section and hence the result shown here are important in reference to decay path and structure information of $^{228}Th^{*}$ nucleus.

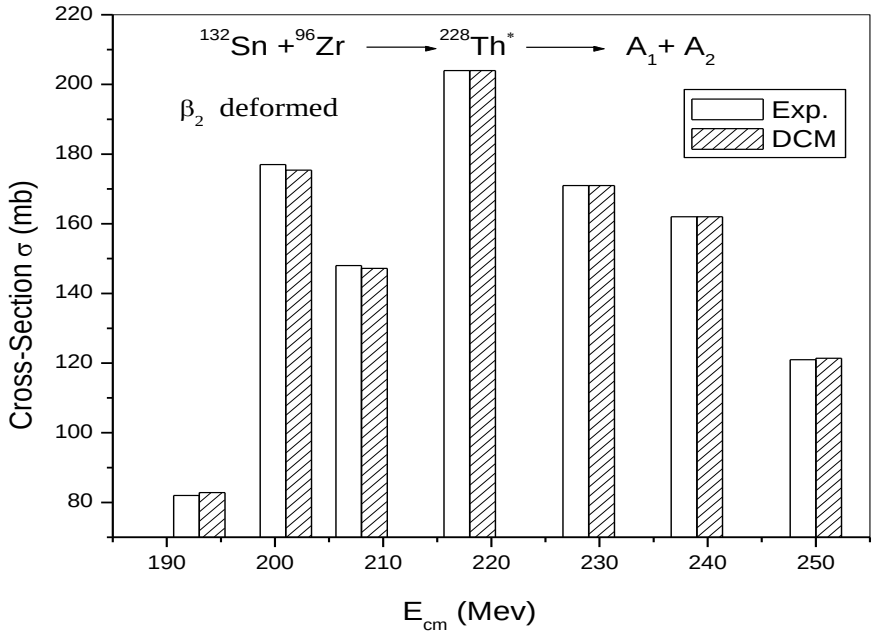

Fig.3.9 Comparison of experimental and DCM calculated cross-section for the decay of $^{228}Th^{*}$ as a function of centre-of-mass energy E_{cm}.

From fig.3.9, a comparison between the experimentally reported cross-section and the DCM calculated cross-section as a function of centre-of-mass energies can be drawn. With the help of neck-length parameter ΔR, the experimental cross-sections have been nicely fitted for all energies with quadrupole (β_2) deformations included. Hence, in framework of DCM the decay of $^{228}Th^{*}$ is studied well, which helps in concluding the dynamical aspect of this reaction.

In summary, the capture cross-section of $^{228}Th^{*}$ formed in $^{132}Sn+^{96}Zr$ reaction are fitted nicely in the framework of DCM. Fission is the main decay mode for this reaction and ER channel contribute negligibly small. The neck-length parameter decreases with increase in energy of incident beam and fission distribution is clearly asymmetric for β_2-deformed choice of fragments and for spherical fragmentation at lower incident energies. However, at higher incident energies the symmetric fragments also start contributing for spherical case. The penetrability do not contribute much towards structural information of compound system and the same is done via. preformation probability. It will be of further interest to account for non-compound nucleus components in decay of $^{228}Th^{*}$ formed in radioactive ^{132}Sn beam and to investigate the concept of fusion enhancement or fusion hindrance in context of experiment [1].

References

[1] A. M. Vinod Kumar etal. Phys. Rev. C 78, 054608 (2008).

[2] R. Kumar & M. K. Sharma Phys. Rev. C 85, 054612 (2012) ; D. Jain, R. Kumar, M. K. Sharma & R.K Gupta, Phys. Rev. C 85, 024615 (2012).

[3] M. K. Sharma, G. Sawhney, R. K. Gupta, W. Grenier, J.Phys.G:Nucl.Part.Phys. 38 105101 (13pp) (2011); K. Sandhu, M. K. Sharma, R. K. Gupta, Phys. Rev. C 85 024604 (2012).

[4] B. B. singh. M. K. Sharma and R. K. Gupta, Phys. Rev. C 77 054613 (2008); M. Kaur, R. Kumar and M. K. Sharma Phys. Rev. C 85 014609 (2012); M. Kaur, M. K. Sharma Phys. Rev. C 85 054605 (2012).

[5] R. K. Gupta, M. Balasubramaniam, R. Kumar, N. Singh, M. Mahhas, and W. Greiner, J. Phys. G: Nucl. Part. Phys. C 31, 631 (2005); M. Manhas and R. K. Gupta, Phys. Rev. C 72, 024606 (2005).

[6] R. K. Gupta, M. Manhas, G. MÄunzenberg, and W.Greiner, Phys. Rev. C 72, 014607 (2005).